MAX-PLANCK-INSTITUT FÜR PHYSIK
WERNER-HEISENBERG-INSTITUT

MPI-PhE 93-12
June 1993

ATLAS MUON - No. 24

High-precision drift tubes

Walter Blum

Abstract

When drift tubes are used for high-precision coordinate measurements there are some limitations to the achievable accuracy of an individual tube. In this paper I try to estimate the limits caused by an imperfect geometry of the tube, by an uncertainty in the knowledge of the magnetic field, and by the ionization and diffusion of typical gases, taking into account the gas density.

80805 München · Föhringer Ring 6

High-precision drift tubes

Walter Blum

Abstract

When drift tubes are used for high-precision coordinate measurements there are some limitations to the achievable accuracy of an individual tube. In this paper I try to estimate the limits caused by an imperfect geometry of the tube, by an uncertainty in the knowledge of the magnetic field, and by the ionization and diffusion of typical gases, taking into account the gas density.

Table of Contents

1. Electrostatics of perfect and of imperfect drift tubes

If a 'proportional tube' is used for a coordinate measurement by recording the drift time of ionization electrons to the wire, one has a 'drift tube'. Whether the signal at the wire is created by a proportional avalanche — as the original name suggests — or by a self-quenching streamer, the drift velocity and the electric field between the two conductors must be very well known if one wants to exploit the intrinsic accuracy of this device.

Deviations from the ideal geometry of two concentric circular cylinders are caused by displaced wires or deformed walls. In this section we discuss the electric field arising in an eliptical right cylinder and in a hexagonal right cylinder with the wire in the centre, and the field arising in a circular right cylinder with the wire off-centre. Since we are dealing with relatively small deviations our method is a perturbation calculation in the first order of the linear deviation.

A general method of determining the solution of Laplace's equation

$$\nabla^2 \Phi = 0 \tag{1.1}$$

for the potential Φ in the charge-free space between two conductors is found in my old college book [1]. After separating variables by writing

$$\Phi(r, \varphi, z) = R(r)\, \phi(\varphi)\, Z(z)\,, \tag{1.2}$$

we have in cylindrical coordinates

$$\frac{1}{rR}\frac{\partial}{\partial r}\left(r\frac{\partial R}{\partial r}\right) + \frac{1}{r^2\phi}\frac{\partial^2 \phi}{\partial \varphi^2} + \frac{1}{Z}\frac{\partial^2 Z}{\partial z^2} = 0 \tag{1.3}$$

Assuming $Z(z) = \text{const} = 1$, the second term is equated to the constant $-\nu^2$ so that

$$\frac{d^2\phi}{d\varphi^2} = -\nu^2 \phi \tag{1.4}$$

whose solutions are

$$\phi(\varphi) = C_\varphi' \cos \nu\varphi + C_\varphi'' \sin \nu\varphi \qquad \text{if } \nu \neq 0 \qquad (1.5)$$

or

$$\phi(\varphi) = C_\varphi' \varphi + C_\varphi'' \qquad \text{if } \nu = 0. \qquad (1.6)$$

The radial part becomes the Euler-Cauchy equation

$$r\frac{d}{dr}\left(r\frac{dR}{dr}\right) - \nu^2 R = 0 \qquad (1.8)$$

If $\nu = 0$, the solution is given by

$$R(r) = C_r' \ln r + C_r'' \; . \qquad (1.9)$$

1.1 Perfect drift tube

The potential between two coaxial cylinders is a straight application of (1.9). When the outer cylinder (radius b) is on ground and the wire (radius a) on positive potential U, one determines the coefficients to be given by $C_\varphi' = 0$, $C_r'' = - C_r' \ln b$ and $C_r' C_\varphi'' \ln (a/b) = U$ so that

$$\phi = \frac{U}{\ln(a/b)} \ln\left(\frac{r}{b}\right) \qquad (1.10)$$

The electric field is directed radially outwards, and

$$E_r = -\frac{\partial \phi}{\partial r} = \frac{U}{\ln(b/a)} \frac{1}{r} \qquad (1.11)$$

Another way to calculate E_r is using Gauss' theorem according to which

$$E_r = \frac{\lambda}{2\pi \varepsilon_0} \frac{1}{r} \qquad (1.12)$$

where λ is the linear charge density on the wire; the value of ε_0 is 8.856×10^{-12} As/Vm. Therefore, the capacitance per unit length of tube is given by

$$C = \frac{\lambda}{U} = \frac{2\pi\varepsilon_0}{\ln(b/a)} \tag{1.13}$$

1.2 Displaced wire

1.2.1 Solution of the electrostatic problem

Let the wire be displaced from the tube centre by the distance d in the negative y-direction (Fig. 1.1). The wire defines the centre of the coordinate system so that the first boundary con-

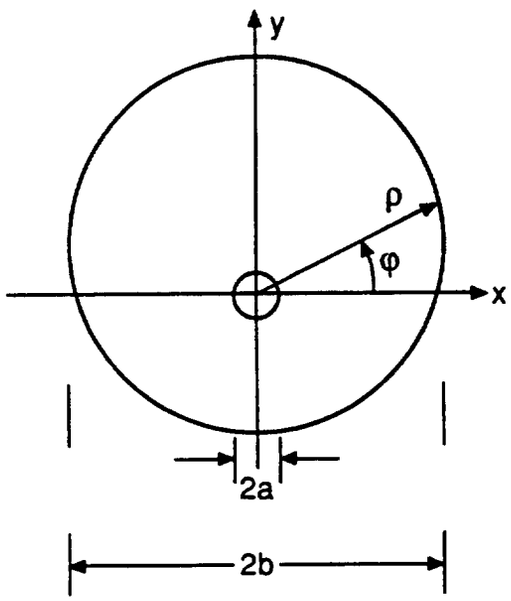

Fig. 1.1. Geometry of displaced wire

dition is

$$\Phi(a) = U \qquad \text{independent of } \varphi \tag{1.14}$$

We must express the second boundary by the radius vector as a function of φ. The exact expression is

$$\rho = d\sin\varphi + b\sqrt{1 - \left(d^2/b^2\right)\left(1 - \sin^2\varphi\right)}\,, \tag{1.15}$$

but we are only interested in small wire displacements. To first order in d/b we have the boundary at

$$\rho = b + d \sin \varphi , \tag{1.16}$$

and the second boundary condition is

$$\Phi (\rho) = 0 . \tag{1.17}$$

Now we must determine the various coefficients using (1.14) and (1.17). To the first order in d/b, we have solutions for $\nu = 0$ and $\nu = 1$, and the most general solution is

$$\Phi = (C_r^{0'} \ln r + C_r^{0''}) C_\varphi^{0''} + (C_r^{1'} r + C_r^{1''} / r) (C_\varphi^{1'} \cos \varphi + C_\varphi^{1''} \sin \varphi) \tag{1.18}$$

Inserting (1.14), we have to require

$$(C_r^{1'} a + C_r^{1''} / a) = 0 \tag{1.19}$$

which implies that $C_r^{1''}$ can be neglected against $C_r^{1'}$ for the entire space except in the immediate vicinity of the wire surface.

When inserting (1.17) and (1.16) into (1.18), we make use of the relation

$$\ln (b + d \sin \varphi) = \ln b + (d/b) \sin \varphi,$$

which holds to first order in d/b. This determines the constants $C_r^{0'}$, $C_r^{0''}$ and $C_\varphi^{0''}$ as in the case (1.10) of the perfect tube. Comparing factors that multiply the sin φ terms, we find

$$C_\varphi^{0''} C_r^{0''} (d/b) + C_r^{1'} b C_\varphi^{1''} = 0$$

or

$$C_r^{1'} C_\varphi^{1''} = -\frac{d}{b^2} \frac{U}{\ln(a/b)} \tag{1.20}$$

whereas $C_\varphi^{1'} = 0$. This produces the solution, in first order of d/b equal to

$$\Phi(r,\varphi) = \frac{U}{\ln (a/b)} \ln\left(\frac{r}{b}\right) - \frac{U}{\ln (a/b)} \frac{d}{b} \frac{r}{b} \sin \varphi \tag{1.21}$$

The perturbing potential Φ_1 caused by the wire displacement is given by the second term. Using $y = r \sin \varphi$, the field perturbation is calculated to be

$$\left(E_1\right)_y = -\frac{\partial \Phi_1}{\partial y} = -\frac{U}{\ln(b/a)}\frac{d}{b^2}$$
$$\left(E_1\right)_x = \left(E_1\right)_z = 0 \qquad (1.22)$$

It describes a constant field directed towards negative y, whose magnitude is (d/b) times the value of the unperturbed field (1.11) at the wall.

For the use in Sect. 1.2.3 we also record the value of $(E_1)_y$ on the wire surface (r = a). Starting from (1.19) without the previous simplification $C_r^{1"} = 0$, the correct perturbation potential is

$$\Phi_1(a) = \frac{U}{\ln(a/b)}\frac{d}{b^2}\left(r - \frac{a^2}{r}\right)\sin\varphi = 0 \quad ; \qquad (1.23)$$

the field in y-direction equals

$$\left(E_1(a)\right)_y = -\frac{\partial \Phi_1}{\partial y} \quad (\text{evaluated at } r = a)$$

$$= -\frac{U}{\ln(b/a)}\frac{2d}{b^2}\sin^2\varphi$$

Averaging over φ we have an average extra field on the wire surface equal to

$$\langle\left(E_1(a)\right)_y\rangle = -\frac{U}{\ln(b/a)}\frac{d}{b^2} \qquad (1.24)$$

The average field on the wire surface is as large as the field perturbation (1.22) throughout the volume.

1.2.2 Gravitational sag

The main reason for wire displacement is the weight of the wire. Even when strung with a pulling force T close to the breaking limit, wires in several metre long tubes will experience a gravitational sag that is large in comparison with the achievable accuracy of drift tubes.

In order to derive a formula for the amount of the bowing we introduce the coordinates y (downwards) and x (horizontal). We note that on every length element dx the weight of the wire is

$$\rho\, g\, Q\, dx \tag{1.25}$$

(ρ = density, Q = cross-sectional area of the wire, g = 981 cm/s^2). It must be compensated by the vertical component of the tension at this point, which is equal to the difference of the slopes at the two ends of the interval dx, multiplied by the pulling force T:

$$-T\,[y'(x+dx) - y'(x)] \tag{1.26}$$

where the primes denote the first derivative. In this approximation we have assumed that the pulling force is the same for all x, the variation due to the weight of the wire being negligible for practical tubes.

Combining (1.23) and (1.24), one has the differential equation

$$-y'' = C = \rho\, g\, Q / T \tag{1.27}$$

with the solution

$$y = -(C/2)\, x^2 + C_1\, x + C_2. \tag{1.28}$$

Specifying that y = 0 at x = $\pm$ L/2 determines the coefficients C_1, C_2, and the solution becomes

$$y = \frac{C}{2}\left(\frac{L^2}{4} - x^2\right) \tag{1.29}$$

The point of the maximum excursion is the sagitta, equal to

$$s = y(0) = \frac{C\,L^2}{8} = \frac{\rho\, g\, Q\, L^2}{8\,T}. \tag{1.30}$$

The ratio T/Q is limited by the material properties of the wire. For example, a 1 m long copper-beryllium wire strung at 500 N/mm^2 — roughly 50% of the elastic limit of the hard alloy — will sag by 22 μm.

1.2.3 Electrostatic force on the sagged wire

The displacement of the wire creates an average field (1.24) which acts on the electric charge of the wire and produces a force which tends to increase the displacement.

The differential equation (1.27) needs to be complemented by a term which represents the electrostatic force per unit wire length. This is given by the product

$$\lambda \; < (E_1 (a))_y > ,$$

where λ is given by (1.12) in terms of the unperturbed field, and $< (E_1 (a))_y >$ is given by (1.24) and is proportional to the displacement y. The electrostatic force, like gravity, points downwards and leads to a positive term on the right-hand side of (1.27), whereas $y'' < 0$. Therefore, the differential equation is

$$y'' + k^2 y + C = 0 \tag{1.31}$$

with $C = \rho g Q/T$ and $k^2 = 2\pi \varepsilon_0 E_0^2(b) / T$. The value of k is plotted against $E_0(b)$ and T in Fig. 1.2.

The general solution of (1.31) is

$$y = C_1 \cos kx + C_2 \sin kx - C/k^2 \tag{1.32}$$

When specifying $y(\pm L/2) = 0$, the coefficients C_1, C_2 are determined, and the solution becomes

$$y = \frac{C}{k^2} \left(\frac{1}{\cos (kL/2)} \cos kx - 1 \right) \tag{1.33}$$

The electrostatic force has changed the form of the wire from the parabola (1.29) to the cosine function (1.33).

The new sagitta is

$$s_k = y(0) = \frac{C}{k^2} \left(\frac{1}{\cos (kL/2)} - 1 \right) \tag{1.34}$$

This means the electrostatic force has increased the sagitta (1.30) by the factor

$$\frac{s_k}{s} = \frac{8}{k^2 L^2} \left(\frac{1}{\cos (kL/2)} - 1 \right) \tag{1.35}$$

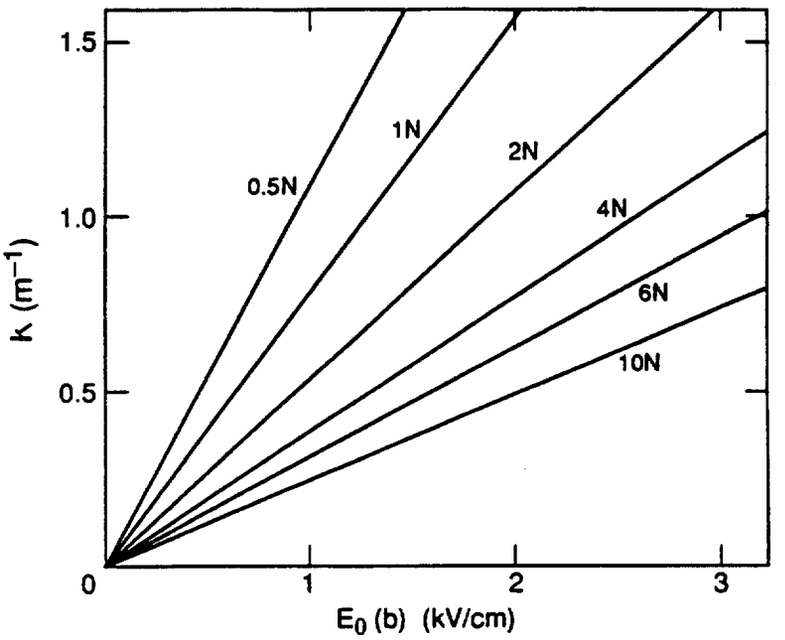

Fig. 1.2. **Value of the constant k in (1.31), relevant for the electrostatic amplification of the gravitational sag, as a function of the electric field $E_0(b)$ at the tube wall, for various wire pulling forces T**

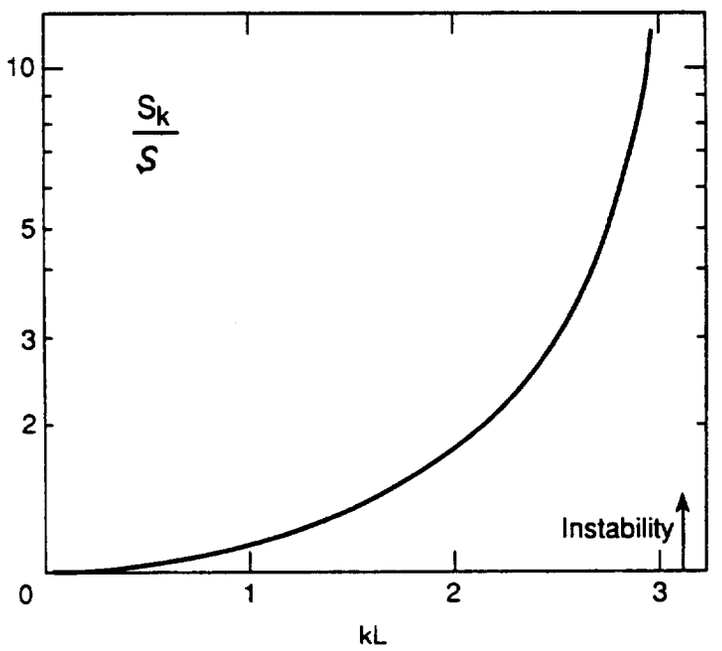

Fig. 1.3. **Electrostatic amplification factor of the gravitational sag, as a function of kL, according to (1.35)**

As the product kL approaches the value of π, the excursion tends to infinity, and the wire is no longer in a stable position. For example, the gravitational sag of a wire strung with one N inside a 4 m long tube will be amplified by a factor s_k/s of 1.8 if the field at the wall is $E_0(b)$ = 500 V/cm, and the point of instability is reached at $E_0(b)$ = 750 V/cm. In Fig. 1.3 we plot s_k/s as a function of kL.

1.3 Elliptical wall

Let the wire (radius a) be in the centre of the ellipse with half-axes b in x-direction and c along y. Defining a mean wall radius R

$$R = (b + c) / 2 \tag{1.36}$$

and the shape parameter $|\beta| << 1$,

$$\beta = (b - R) / R \tag{1.37}$$

the tube wall is given to first order in β by the length ρ of the radius vector as a function of φ:

$$\rho = R (1 + \beta \cos 2\varphi) . \tag{1.38}$$

(Previously R was used (1.2) to mean a potential function.)

Referring to (1.5) and (1.6), we have solutions for $\nu = 0$ and $\nu = 2$; the most general solution is

$$\Phi = (C_r^{0'} \ln r + C_r^{0''}) C_\varphi^{0''} + (C_r^{2'} r^2 + C_r^{2''} / r^2) (C_\varphi^{2'} \cos 2\varphi + C_\varphi^{2''} \sin 2\varphi) \tag{1.39}$$

The two boundary conditions are

$$\Phi (a) = U \tag{1.40}$$

and

$$\Phi (\rho) = 0, \text{ independent of } \varphi \tag{1.41}$$

From (1.40) we conclude

$$(C_r^{2'} a^2 + C_r^{2''} / a^2) = 0 \tag{1.42}$$

which implies that the term containing $C_r^{2''}$ can be neglected against $C_r^{2'}$ except in the immediate vicinity of the wire.

When inserting (1.41) and (1.38) into (1.39) we make use of the relation

$$\ln [R(1 + \beta \cos 2\varphi)] = \ln R + \beta \cos 2\varphi \tag{1.43}$$

which holds to first order in β. The constants $C_r^{0'}$, $C_r^{0''}$ and $C_\varphi^{0''}$ are determined as in the case of the perfect tube. Comparing factors that multiply the cos 2φ terms, we find

$$C_r^{0'} C_\varphi^{0''} \beta + C_r^{2'} C_j^{2'} R^2 = 0 \tag{1.44}$$

and $C_\varphi^{2''} = 0$. This defines the coefficients

$$C_r^2 C_\varphi^{2,} = - \frac{\beta}{R^2} \frac{U}{\ln (a/R)} \tag{1.45}$$

Therefore the solution , for $r^2 >> a^2$ and to first order in β, is the following:

$$\Phi(r,\varphi) = \frac{U}{\ln (a/R)} \ln\left(\frac{r}{R}\right) - \frac{U}{\ln (a/R)} \beta \frac{r^2}{R^2} \cos 2\varphi \tag{1.46}$$

The perturbing potential Φ_2 caused by the deformation of the tube is given by the second term. It describes a quadrupole field: using Cartesian coordinates, $x = r \cos \varphi$ and $y = r \sin \varphi$ the perturbing field $\mathbf{E_2}$ is given by

$$\Phi_2(x,y) = \beta \frac{U}{\ln (R/a)} \frac{x^2 - y^2}{R^2} \tag{1.47}$$

$$(E_2)_x = -\beta \frac{U}{\ln (R/a)} \frac{2x}{R^2}$$

$$(E_2)_y = +\beta \frac{U}{\ln (R/a)} \frac{2y}{R^2} \tag{1.48}$$

$$(E_2)_z = 0$$

The magnitude of $\mathbf{E}_2$ is constant around the circumference of the wall and equal to 2β times the unperturbed field $\mathbf{E}_0$ at the wall, compare Fig. 1.4.

1.4 Hexagonal wall

The hexagonal wall can be described in cylindrical coordinates by the condition

$$\rho = \frac{b}{\left|\cos(\varphi \bmod 60^\circ)\right|} \tag{1.49}$$

where b is the radius of the inscribed circle of the hexagon.

In order to apply the method outlined in the beginning of this Section 1, $r(\varphi)$ has to be expressed in terms of a power series in $\cos \nu\varphi$ and $\sin \nu\varphi$. Here we are satisfied with the lowest term, and the general symmetry of the problem suggests we define a $\rho^*(\varphi)$ by

$$\rho^*(\varphi) = b\,(1 + \delta - \varepsilon \cos 6\varphi) \tag{1.50}$$

We let the two coefficients δ and ε be determined by a principle of least squares:

$$\chi^2 = \int_{-30}^{+30} \left[\rho(\varphi) - \rho^*(\varphi)\right]^2 d\varphi = \text{minimum} \tag{1.51}$$

Inserting (1.49) and (1.50) into (1.51) and doing five integrals, one obtains

$$\begin{aligned} \delta &= 0.046 \quad \text{and} \\ \varepsilon &= 0.056. \end{aligned} \tag{1.52}$$

There is some arbitrariness in using condition (1.51), and we imagine δ and ε to have some uncertainty due to this reason. An even larger uncertainty arises from the actual form of the 'hexagon' which in one practical case is the product of a machine that folds a plastic foil. Account of these uncertainties will be taken in Sect. 3.4.3. We define the effective radius R,

$$R = b\,(1 + \delta) = 1.046\,b \tag{1.53}$$

Then in first order of δ, ε,

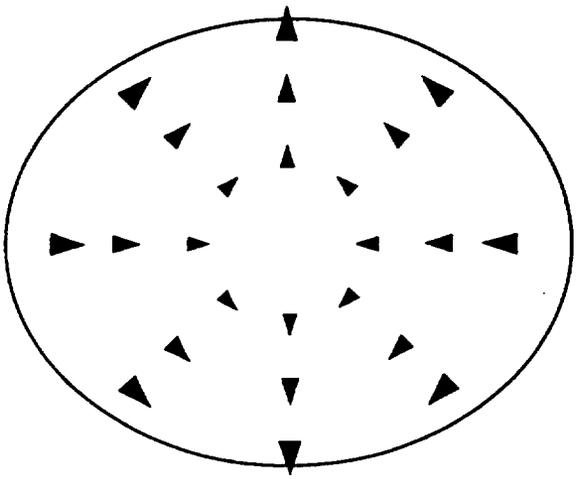

Fig. 1.4. Graphical representation of the perturbing field E_2 inside an elliptical tube. The area of each arrow is proportional to the magnitude $|E_2|$

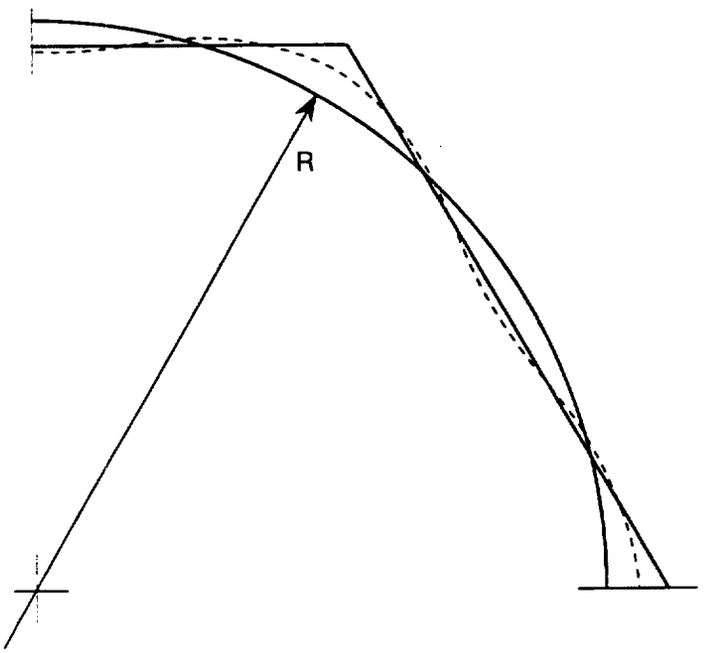

Fig. 1.5 Approximation of the hexagon by (1.54)

$$\rho^* = R\,(1 - \varepsilon \cos 6\varphi). \tag{1.54}$$

This approximation of the hexagon is illustrated in Fig. 1.5. The most general solution contains the sixth power of the radius and is given by

$$\Phi = (C_r^{0'} \ln r + C_r^{0''})\, C_\varphi^{0''} + (C_r^{6'} r^6 + C_r^{6''} / r^6)\,(C_\varphi^{6'} \cos 6\varphi + C_\varphi^{6''} \cos 6\varphi)$$

The two boundary conditions are

$$\Phi(a) = U \tag{1.56}$$

$$\Phi(\rho^*) = 0 \tag{1.57}$$

Going through the same steps as before yields

$$\Phi = \Phi_0 + \Phi_6 = \frac{U}{\ln (a/R)} \ln\left(\frac{r}{R}\right) - \frac{U}{\ln (a/R)}\, \varepsilon \left(\frac{r}{R}\right)^6 \cos 6\varphi \tag{1.58}$$

The potential Φ_6 describes the difference of the field configurations of the hexagonal and the circular cylindrical tubes. The field $\mathbf{E_6}$ has the following radial and tangential components:

$$(E_6)_r = -\frac{\partial \Phi_6}{\partial r} = \frac{U}{\ln (a/R)}\, \frac{6\varepsilon}{R} \left(\frac{r}{R}\right)^5 \cos 6\varphi \tag{1.59}$$

$$(E_6)_\varphi = -\frac{1}{r}\frac{\partial \Phi_6}{\partial \varphi} = -\frac{U}{\ln (a/R)}\, \frac{6\varepsilon}{R} \left(\frac{r}{R}\right)^5 \sin 6\varphi \tag{1.60}$$

We note that the magnitude of this high-multipole field is independent of φ; in comparison with the field at the wall of the perfect tube, it is smaller by the factor

$$\frac{|E_6(r)|}{|E_0(R)|} = 6\varepsilon \left(\frac{r}{R}\right)^5 \tag{1.61}$$

As one goes around, varying φ at constant r, the field $\mathbf{E_6}$ changes its direction and goes through six full revolutions as the wire is surrounded once (Figs. 1.6, 1.7).

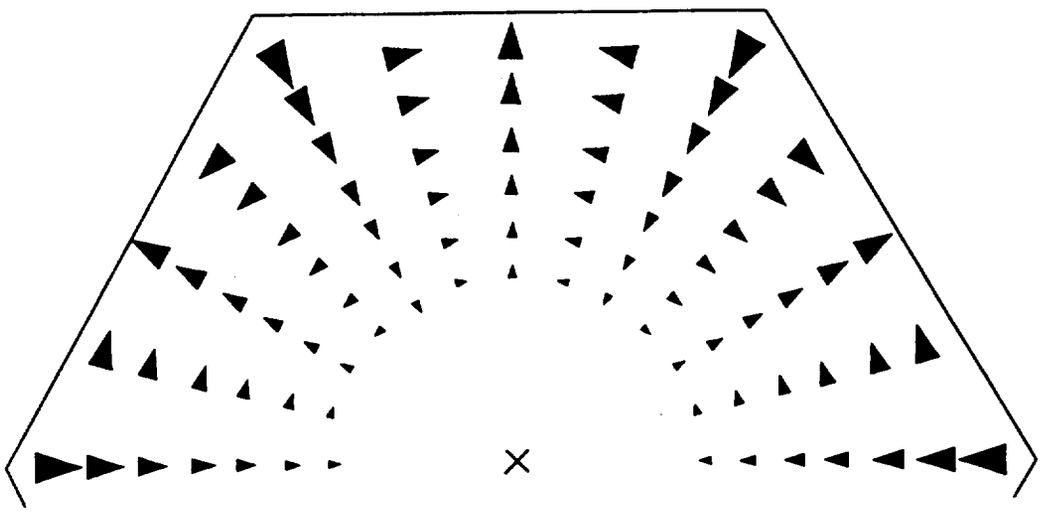

Fig. 1.6. Graphical representation of the perturbing field E_6 inside a hexagonal tube. The area of each arrow is proportional to the magnitude $|E_6|$

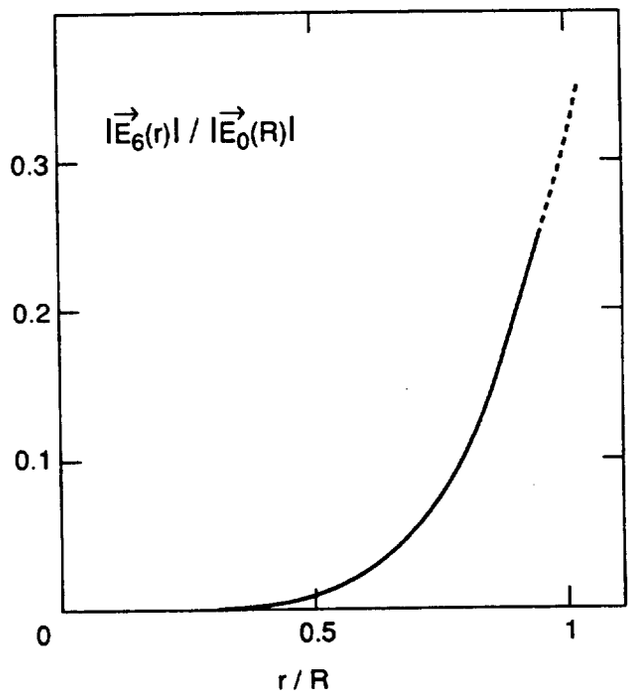

Fig. 1.7. Magnitude of the field E_6 in units of the magnitude of the unperturbed field $E_0(R)$ at the wall of the perfect cylinder, as a function of the relative radius r/R, according to (1.61)

2. Choice of the gas and of the drift field under practical conditions

2.1 Parametrization of the drift velocity

Being proportional to 1/r, the drift field E in a tube is quite inhomogeneous, and for the drift behaviour of the gas in the tube we must consider the variation of the drift velocity u with E. Drift gases exhibit a broad variety of behaviours, and in the end a given gas must be studied on the basis of its measured function u(E).

In order to obtain an overview about possible choices of a gas in the region of low values of E, we describe a typical u(E) by two parameters as rising from zero with mobility μ, then remaining constant at u_0.

$$u(E) = \begin{cases} \mu E & E < E_0 \\ u_0 & E > E_0 \end{cases} \qquad (2.1)$$

The field E_0 is given by $\mu E_0 = u_0$. Let E_0 be reached at radius r_0. The field E_b at the wall is related to r_0 by

$$r_0 = \mu E_b b / u_0 \qquad (2..2)$$

where b is the inner tube radius. The variation of u inside the tube is shown in Fig. 2.1.

2.2 Drift space–time relation

The drift time from any point r to the origin is

$$T(r) = \begin{cases} \displaystyle\int_0^r \frac{dr}{u_0} = \frac{r}{u_0} & (r \le r_0) \\ \displaystyle\int_0^{r_0} \frac{dr}{u_0} + \int_{r_0}^{r} \frac{r\,dr}{\mu E_0 r_0} = \frac{r_0}{2u_0} + \frac{r^2}{2u_0 r_0} & (r \ge r_0) \end{cases} \qquad (2.3)$$

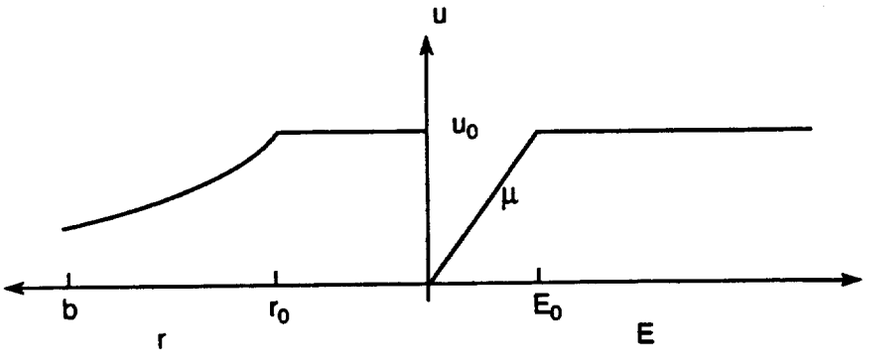

Fig. 2.1 **Drift velocity plotted against the electric field E and against the tube radius r, according to the parametrisation (2.1)**

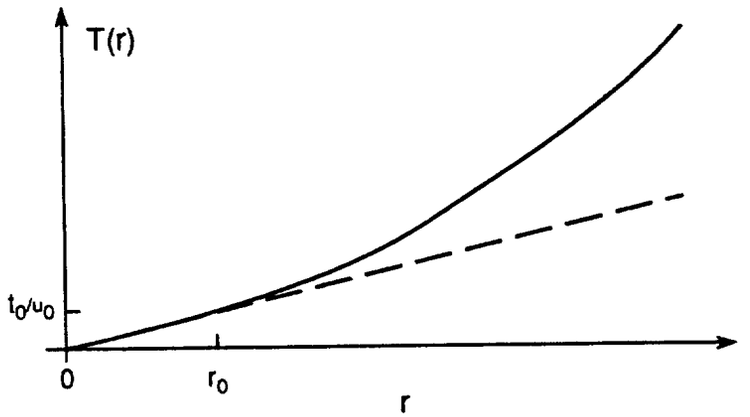

Fig. 2.2. **Drift space–time relation according to (2.3)**

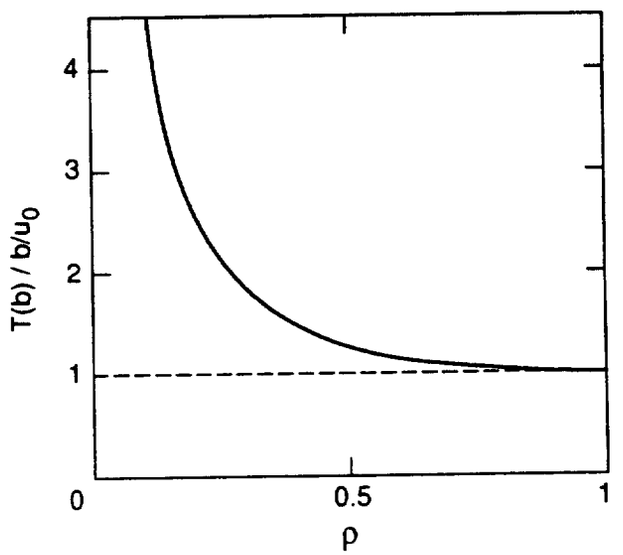

Fig. 2.3. **Maximum drift, expressed in units of b/u_0, as a function of the ρ-parameter, according to (2.4)**

It begins with a part linear in r and continues with a quadratic term, see Fig. 2.2. The maximum drift time T(b) depends on the ratio $\rho = r_0 / b$; for the case that is of practical importance ($r_0 \leq b$), it takes the form

$$T(b) = \frac{r_0}{2u_0} + \frac{b^2}{2u_0 r_0} = \frac{b}{u_0}\left(\frac{\rho}{2} + \frac{1}{2\rho}\right) \tag{2.4}$$

This function is depicted in Fig. 2.3. We observe T(b) to remain almost constant as ρ is decreased from 1 to 0.5, but it quickly rises as ρ is decreased further. For example, $T(b) = 2.1\ b/u_0$ at $\rho = 0.25$.

A small value of $\rho = r_0 / b$ also leads to the unfavourable situation that the drift velocity at the wall of the tube is smaller than it is near the wire by the factor

$$\frac{u_{min}}{u_{max}} = \frac{r_0}{b} \tag{2.5}$$

2.3 Influence of a magnetic field parallel to the wire on the electron drift

With a magnetic field B parallel to the wire, the electrons do not travel on radial approach lines towards the wire, but under an angle ψ which is roughly given by

$$\tan \psi = \omega \tau \tag{2.6}$$

where $\omega = e/m\ B$ is the electron cyclotron frequency and τ is the mean time between collisions of the electrons with the gas molecules. To a good approximation $\omega\tau$ can be calculated using the electron mobility

$$\mu = \frac{e}{m}\tau, \tag{2.8}$$

which results in

$$\omega\tau = \mu B. \tag{2.9}$$

The change in the drift direction makes the electron approach the wire on a curve which is illustrated for three different constant values of $\omega\tau$ in Fig. 2.4. The factor by which the curve is longer than the corresponding straight line is obviously equal to

$$\frac{1}{\cos\psi} = \text{factor of elongation} \tag{2.10}$$

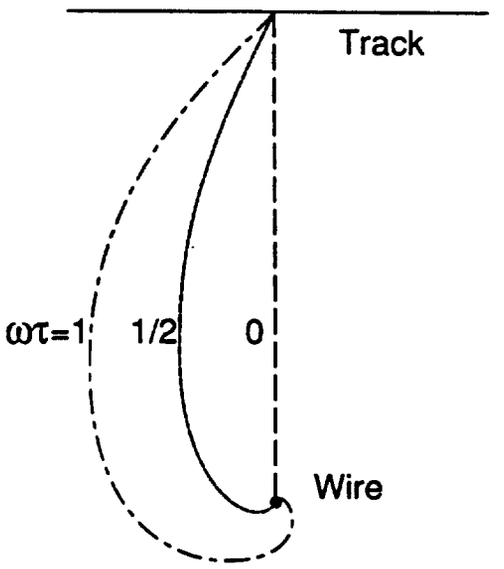

Fig. 2.4. Electron drift paths for various values of $\omega\tau$

When the magnetic field is switched on, the electrons will also have the magnitude of their drift velocity changed from u(E,0) to u(E,B). It is not easy to calculate u(E,B) for the general case, but for the simplification (2.1), progress is possible using Tonks' theorem [2]. It states that the drift velocity will remain the same when switching on B, provided E is changed from E_1 to E_2:

$$u(E_1,0) = u(E_2,B), \tag{2.11}$$

where

$$E_2 = E_1 / \cos\psi \tag{2.12}$$

Using (2.1), this implies a reduction of the mobility by the factor cos ψ in the outer drift region, and no change in the inner one. (There is also a slight change in r_0.)

$$u(E,B) = \begin{cases} \mu(B=0)\ \cos\psi\ E & r \geq r_0 \\ u_0 & r \leq r_0 \end{cases} \tag{2.13}$$

2.4 Limits on drift parameters resulting from an uncertainty in the knowledge of the magnetic field

Although we deal with coordinate measurements and their achievable accuracy only in Sect. 3, we single out one particular source of error to be treated here under the aspect of the choice of the drift parameters. If the magnetic field exhibits some inhomogeneity it may happen that its value at some particular point is only known inside some latitude ΔB. The effects described in Sect. 2.3 then lead to an uncertainty in the arrival time and hence in the measured coordinate. This uncertainty may become large for small values of $\cos\psi$. Therefore, there is a necessity to restrict the value of ψ by a proper choice of drift parameters.

In the regime of constant mobility ($r \geq r_0$) the drift time is stretched by the constant factor $1/\cos^2\psi$, in the regime of constant velocity ($r \leq r_0$) the time is stretched by the variable factor $1/\cos\psi$ whose dependence on the radius is given by

$$\cos^2\psi = 1/(1+\omega^2\tau^2) \tag{2.14}$$

and

$$\omega\tau(r) = B\,\mu(r) = B\,\frac{u_0}{E(r)} = \frac{Bu_0 r}{E_b b} \qquad (r \leq r_0) \tag{2.15}$$

An uncertainty in the knowledge of ω results in an error Δr in the coordinate. We will limit ourselves to an estimate of Δr in the outer region. Since the coordinate is stretched by a constant factor $1/\cos^2\psi$, we have

$$(r - r_0)' = (r - r_0)/\cos^2\psi = (r - r_0)\left(1 + \omega^2\tau_0^2\right) \tag{2.16}$$

$$\Delta r = \omega\frac{dr'}{d\omega}\frac{\Delta\omega}{\omega} = 2(r - r_0)\,\omega^2\tau_0^2\frac{\Delta\omega}{\omega} = 2(r - r_0)\,\omega^2\tau_0^2\frac{\Delta B}{B} \qquad (r \geq r_0) \tag{2.17}$$

Here we have neglected the change in r_0 due to the B-field.

Since the r.m.s. average of $(r-r_0)$ for r between r_0 and b is $(1/\sqrt{3})\,(b-r_0)$, we find

$$(\Delta r)_{rms} = \frac{2}{\sqrt{3}}\,\omega^2\tau_0^2\,(b - r_0)\frac{\Delta B}{B} \qquad (r \geq r_0) \tag{2.18}$$

The smaller part of Δr which arises in the region $r \leq r_0$ can be worked out using (2.15), and can be added to (2.18). For the practical purpose of establishing a limit on the drift parameters, we work with the slightly conservative but simpler relation

$$\frac{(\Delta r)_{rms}}{b} = \frac{2}{\sqrt{3}} \omega^2 \tau_0^2 \frac{\Delta B}{B} \tag{2.19}$$

It implies that the Lorentz angle (c.f. (2.6)) should not exceed a value ψ_{max} which is given by the relative uncertainty $\Delta B/B$ in the knowledge of the magnetic field and the allowed coordinate measuring error Δr. This also defines, via the relation (2.9), an upper limit for the electron mobility μ. The upper limit μ_{max} on the mobility imposed by (2.19) and (2.9) is

$$\mu_{max} = \sqrt{\frac{\sqrt{3}(\Delta r)_{rms}/b}{2\,\Delta B/B}} \frac{1}{B} \tag{2.20}$$

Using a numerical example relevant for the ATLAS air core toroid, we estimate for a maximum allowed relative error of this kind of $\Delta r/b$ = 15 μm / 15 mm, and a typical field of B = 1 T, the limits quoted in Table 2.1.

Table 2.1. Limits imposed on the Lorentz angle and the electron mobility by an uncertainty in the knowledge of the magnetic field, according to (2.19), using $(\Delta r)_{rms}/b$ =15 μm / 15 mm and B = 1 T.

$\Delta B / B$	$\omega\tau_0$	ψ_{max} (deg)	μ [cm^2/(μs kV)]
0.10	0.09	5.3	0.9
0.05	0.13	7.4	1.3
0.02	0.21	12	2.1
0.01	0.29	16	2.9

2.5 Summary — the difficulty of making the drift velocity high and uniform

A high drift velocity over the largest possible range of radii is desirable because it makes the maximum drift time shorter, the drift space–time relation more linear, and the measured coordinate less dependent on variations of field or gas density. Assuming a general behaviour of the drift velocity as in Fig. 2.1, this implies one should choose a high electron mobility μ and/or a high field E. However, the value of μ is limited by the size of the admissible

influence of the magnetic field on the measured coordinate, see (2.20) and the numerical example worked out in Table 2.1. If one fixes some admissable value of μ_{max}, one is then led to fix the value of ρ next, see (2.4, 2.5). This leads to a value of the E field at the tube wall that is equal to

$$E_b = \frac{u_0 \rho}{\mu_{max}} \tag{2.21}$$

For example, E_0 has to be as high as 1.2 kV/cm for μ_{max} = 2.1 cm^2 / (μs kV), u_0 = 5 cm/μs and ρ = 0.5.

Such a high field at the tube wall is not practical for tubes with a radius of one or several cm because it requires too high wire potentials. For details, see [6]. In order to reach more practical values of E_b, say 0.4 or 0.6 kV/cm, the product $u_0\rho$ must be reduced correspondingly. Therefore, the drift velocity cannot be simultaneously high and uniform.

3. Coordinate measurement using the drift time, and limitations of the accuracy

3.1 Ionization distribution at the wire

The simple wirte at the centre of a tube detects all the ionization of a track across the tube. After the passage of the particle, some time elapses until the first ionization electron arrives, the last electrons come in the maximum drift time T(b) (c.f. Sect. 2.1) after the moment of the particle passage. The distribution of arrival times t exhibits a characteristic front, which is originally infinitely sharp, followed by a gradual transition into the constant rate of arrival of the distant ionization. The first question of interest is how well this front is defined, given the fact that the ionization happens in discrete clusters of variable size and also that the electrons on their way to the wire are subject to diffusion.

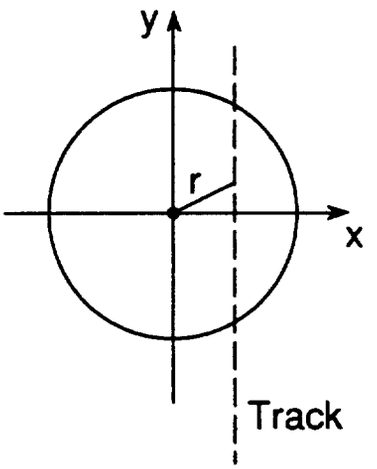

Fig. 3.1. Geometry of a track traversing the circular tube

Referring to Fig. 3.1, the average rate of arrival at the wire is given by the product of the ionization density $\eta = dN/dy$ along the track, the derivative of the track coordinate with respect to the radius, and the drift velocity dr/dt which in turn is a function of t:

$$\frac{dN}{dt} = \eta \frac{dy}{dr} \frac{dr}{dt} \tag{3.1}$$

However, it is simpler to describe the process as a function of r rather than of t — one avoids the use of the time-dependent drift velocity. Therefore we discuss the behaviour of the average 'radial ionization distribution'

$$\frac{dN}{dr} = \eta \frac{dy}{dr} = \eta \frac{r}{\sqrt{r^2+x^2}} \quad . \tag{3.2}$$

In Fig. 3.2 we plot this distribution for five tracks located at various x.

The asymptotic value η at large r depends on the gas and its pressure; for example, η_p is about 42 primary clusters per cm in argon at NTP for extremely relativistic muons. This value is based on the measurement of 27.8 ± 0.3 [3] in the minimum of the ionization curve, times a factor of about 1.5 from the relativistic rise as measured by Lehraus for the total ionization.The relativistic rise of the primary ionization in argon has not been measured, to our knowledge. The total ionization is, roughly speaking, three times larger: $\eta_t \approx 3\,\eta_p$. The expressions (3.1) and (3.2) may refer to either η_p or η_t. η_p is proportional to the gas pressure.

3.2 Fluctuation of the arrival position — primary ionization

One way to visualize the influence of the primary ionization density on the accuracy of the front is to ask at what average distance Δr behind the front one expects the first primary cluster. With reference to Fig. 3.1, the k-th cluster is expected, on average, within the interval

$$\Delta r = \sqrt{x^2+\left(\frac{k}{2\,\eta_p}\right)^2} - x \tag{3.3}$$

where k / η_p is the average track length for k clusters. The curves of Fig. 3.3 show Δr for various k, calculated for argon at NTP as a function of x. As it turns out, the front is very well defined — for a track at x = 1 mm the first cluster comes within 7 μm, the second within 28, the third within 62 μm behind the front. In conclusion, the primary ionization in argon at NTP is dense enough for accuracies well below 100 μm — provided there is sensitivity to the first very few clusters. At higher thresholds the region of reduced accuracy near the wire will extend.

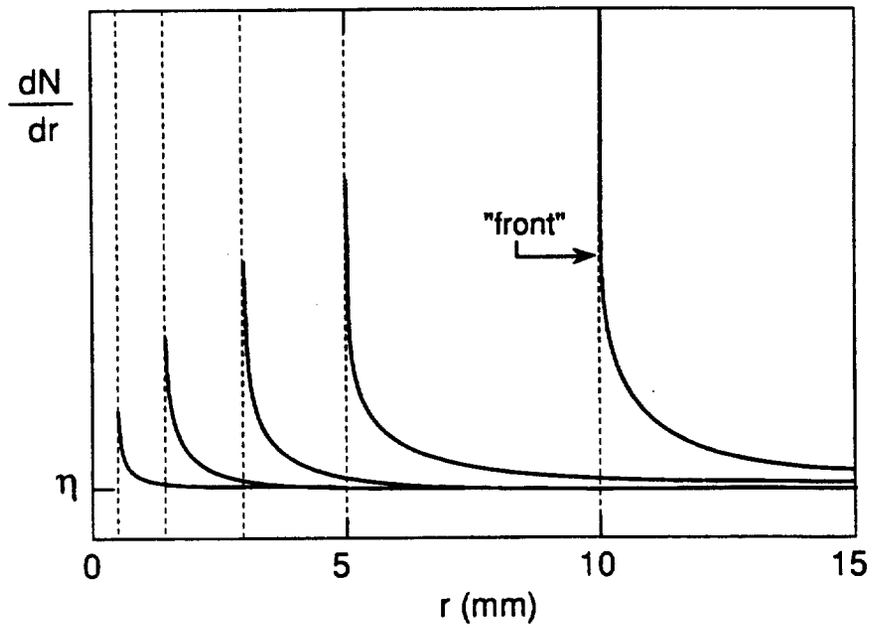

Fig. 3.2. **Radial distribution of ionization according to (3.2), for five tracks at 0.5, 1.5,3,5, and 10 mm distance from the wire**

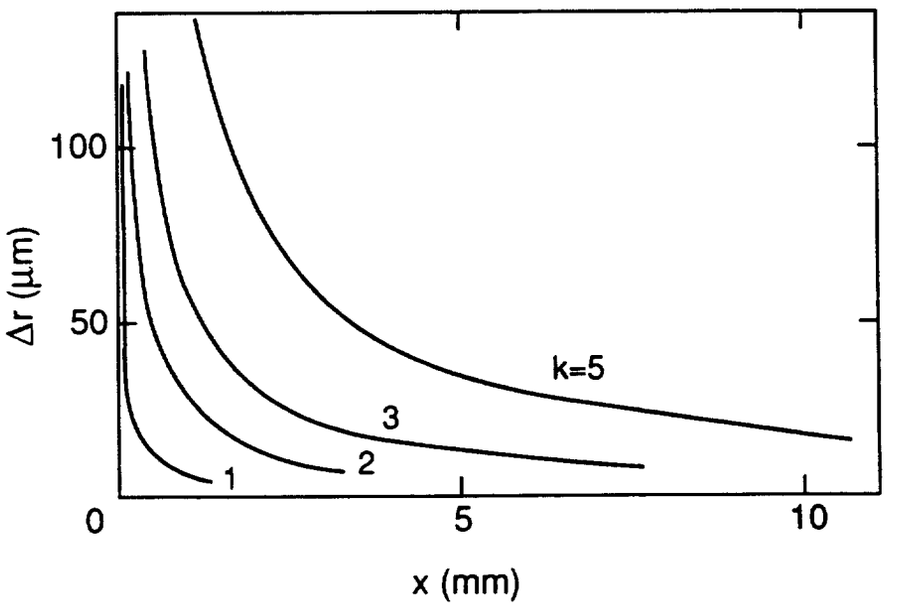

Fig. 3.3. **Average distance Δr of the k–th primary cluster behind the front, as a function of the track–wire distance x, calculated for a primary ionization density of 42/cm, the approximate value for highly relativistic muons in argon gas at NTP**

3.3 Fluctuation of the arrival position — diffusion

The other mechanism to smear out the front of arriving electrons is their diffusion. An analytic description of this smearing process does not exist, and one must involve a numerical simulation. We must take account of the fact that electrons are created in clusters, each electron diffusing independently on its way to the wire.

3.31 Cluster size distribution

The number n_{clus} of electrons created in each primary cluster follows a distribution first calculated by Lapique and Piuz [4]. Their curve was complemented for this paper towards larger n_{clus}, following [5]. The resulting integral distribution is depicted in Fig. 3.4. It is worth noting that very large clusters may occur at low rates — for example, it is 2% probable to exceed 20 electrons. The exact shape of the distribution is not essential for our purpose.

3.3.2 Behaviour of the diffusion

Since the diffusion constant is a function of the electric field the contribution to the width of the single-electron diffusion will be different for every radius. Our interest here is a basic exploration of the statistical factor in the smearing of the electron front, therefore we will characterize the degree of diffusion by a single effective number, σ_1, defined to be the rms width of a single-electron diffusion over 1 cm at NTP of the respective gas mixture. The diffusion of an electron created at some radius r_i and arriving at the wire is accounted for by a random radial shift Δr according to a Gaussian distribution

$$\frac{1}{\sqrt{2\pi}\,\sigma_{(i)}} \exp -\frac{(\Delta r)^2}{\sigma_{(i)}^2} \tag{3.4}$$

with

$$\sigma_{(i)} = \sigma_1 \sqrt{\frac{r_i}{1\ \mathrm{cm}}}\ \sqrt{\frac{1\ \mathrm{bar}}{p}} \tag{3.5}$$

where p is the gas pressure.

3.2.3 Simulation program and results

The purpose of the numerical simulation of the diffusion process is to find the statistical factor which relates the single electron diffusion width to the variation in the space positions of the ensemble of electrons contributing to the signal. This factor depends in our approximation on the track–wire distance and on the ionization characteristics. It is assumed that the k-th arriving electron will trigger the signal. The computer program employed for this purpose is summarized in Table 3.1, results are plotted in Figs. 3.5 to 3.6.

As first examples we treated the cases k=1 and k=10, representative for signal triggers in the limited streamer mode (k=1) and in a typical proportional mode (k=10). An arbitrary and somewhat pessimistic value for the diffusion was chosen as $\sigma_1 = 0.32$ mm/$\sqrt{}$(bar cm). The variance σ^2_{track} of the arrival positions is plotted in Fig. 3.5 against the track–wire distance x for various gas pressures (densities). The contribution of the diffusion is seen in the linearly rising parts of the curves whereas the primary ionization determines the curves at low x.

Three observations are in place. The improvement in the variance with increasing pressure is faster than inversely proportional to the pressure because the number of competing electrons increases with the pressure. The first electron (Fig. 3.5 a) is a good measure of

Table 3.1. Summary of the simulation program to obtain $\langle r_k \rangle$ and σ_k as functions of x, p and σ_1

1. Define x, p, σ_1
2. Compute tracklength l (using tube radius) and primary cluster density η_p
3. Define l η_p random cluster coordinates y_i along track, define radial cluster positions r_i
4. Define for each cluster the diffusion width $\sigma_{(i)}$ using σ_1, p and r_i
5. Define in each cluster n_{clus} electrons according to cluster size distribution
6. Vary each radial electron position by a random number according to a Gaussian with width $\sigma_{(i)}$
7. Order all electrons according to their radial positions
8. Enter radial position of k-th electron into histogram k
9. Repeat steps '3' - '8' 1000 times
10.Obtain average $\langle r_k \rangle$ and rms deviation σ_k of the k-th histogram

position where the ionization statistics is the dominant error source, but it is a bad measure where diffusion is dominant. Vice versa, the tenth electron (Fig. 3.5 b) is a good measure of position where diffusion dominates, and a bad one for ionization.

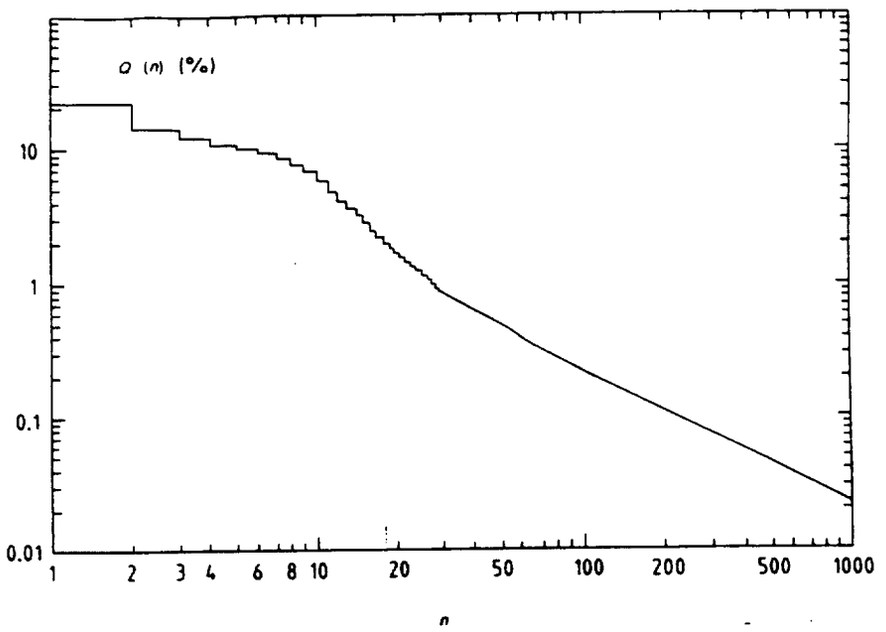

Fig. 3.4. **Integral cluster size distribution Q(n) for highly relativistic particles in argon at NTP, according to [4] and [5]**

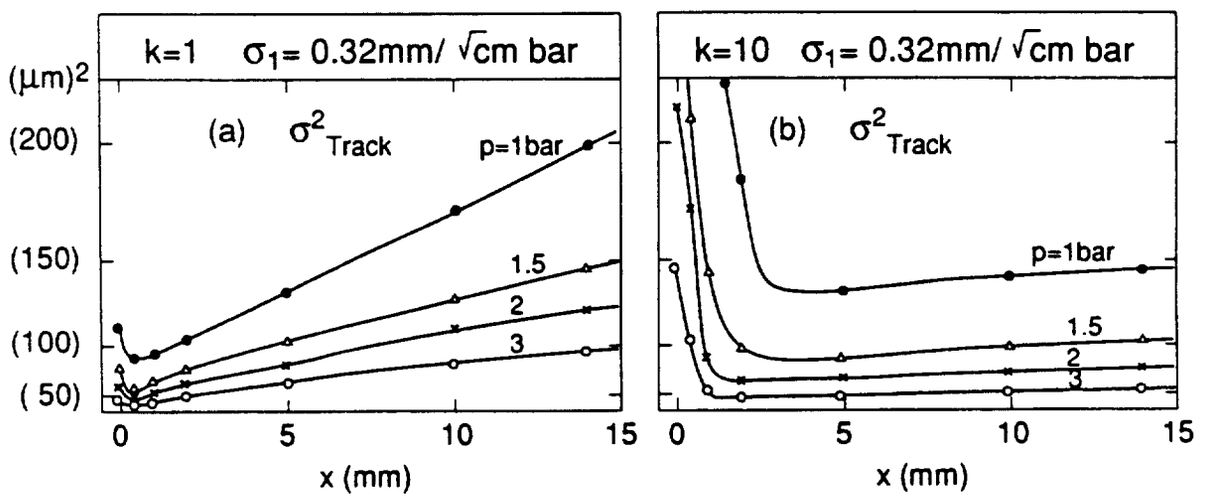

Fig. 3.5. **Track measuring accuracy σ_{track} calculated by the program shown in Table 3.1, for various track–wire distances x and various gas pressures. the diffusion was assumed to be σ_1 =0.32 mm/ $\sqrt{}$(bar cm). (a) trigger from first electron, (b) trigger from 10–th electron**

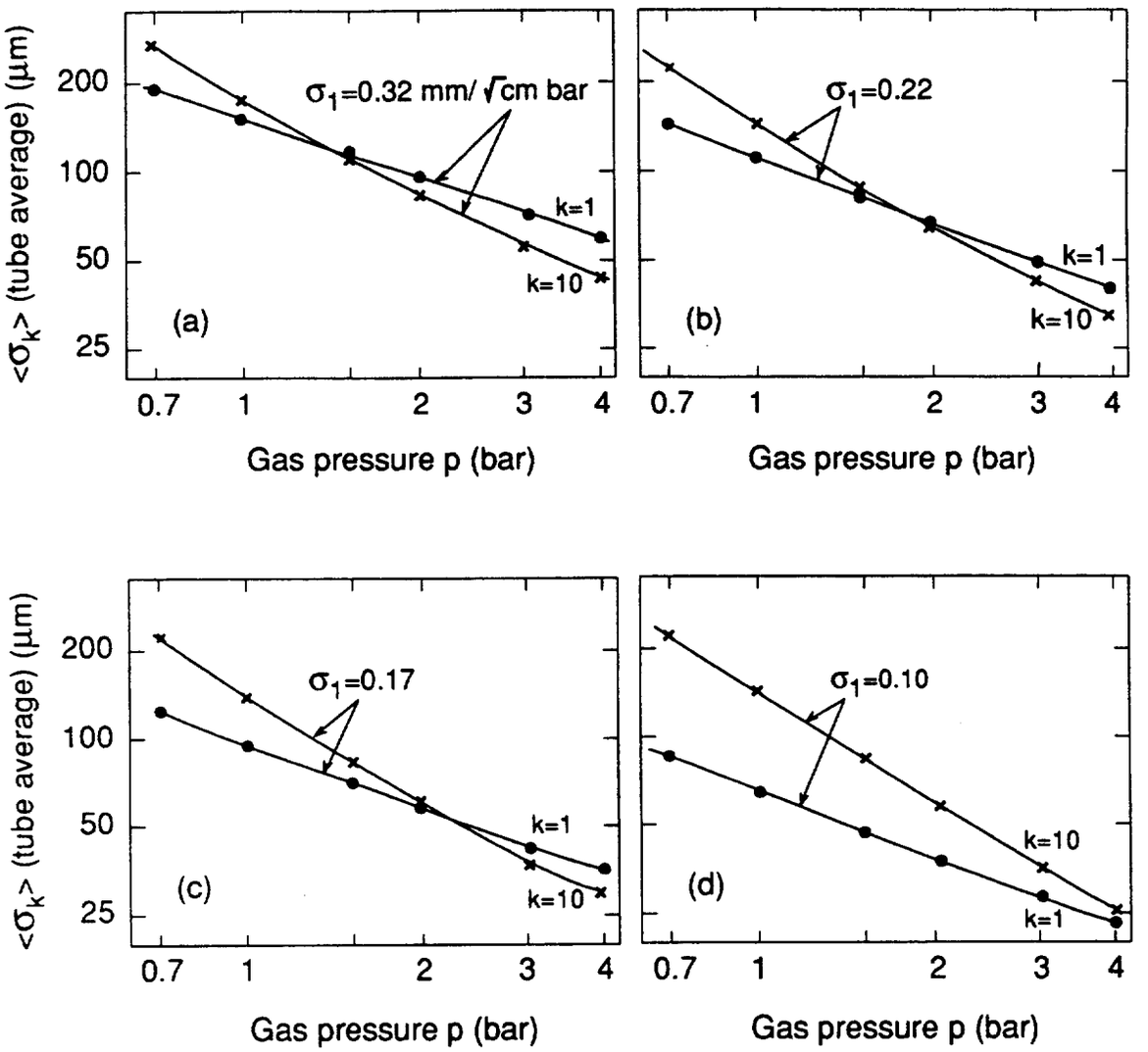

Fig. 3.6. **Tube–averaged track measuring accuracy (r.m.s) as a function of the gas pressure, calculated for k = 1 and k = 10; (a)–(d): four differentvalues of the diffusion quantity σ_1**

In order to arrive at a figure of merit for the full tube the above variances must be averaged over all radii (see also Sect. 3.6). In our example we chose tubes with a diameter of 3 cm. The resulting r.m.s. single track tube accuracy is called $< \sigma_k >$ and is plotted in Fig. 3.6 a as a function of the gas pressure. Analogous curves (Figs. 3.6 b-d) were computed for three other values of diffusion, corresponding to a range of typical gases. One observes the accuracy at low pressures to be better for k=1 than it is for k=10, whereas for high pressures the situation is reversed. The cross-over point moves to higher pressures as the importance of diffusion is diminished.

In summary, within the ranges of diffusion and of threshold studied here we may expect to reach a measurement accuracy better than 50 μm with gas pressures up to a few bar. The curves in Figs. 3.6 b and c gave rise to a more detailed investigation of argon–carbon-dioxide gas mixtures [6]; providing a first definition of the operating point of the ATLAS prototypes.

3.4 Uncertainty in the coordinate measurement caused by variations in the electrostatic boundary conditions

It was shown in Sect. 1 that the displaced wire as well as the elliptically and hexagonally deformed tubes cause certain field distortions. These are relevant for coordinate measurements using the drift time, as long as the drift velocity varies with the field. In drift tubes with their characteristic, large variation of field strength over the drift volume, the drift velocity near the wall is usually proportional to the field strength

$$u = \mu E, \tag{3.6}$$

where μ is the constant mobility. Near the wire, the drift velocity usually varies less with E, but the region of approximately constant μ extends over most of the drift space.

When existing geometrical deformations are ignored there will be an error in the coordinate measurement. We want to compute the shift Δr introduced by each of these field distortions; its value generally depends on the track direction relative to the field distortions. In each case we will select the direction $\hat{y}$ with the largest shift. We also treat the worst case of the drift-velocity field relation by using (3.6) for all radii.

3.4.1 Displaced wire

The disturbing field E_{1y}, in the direction $\hat{y}$ by which the tube centre has been separated from the wire, is, according to (1.22), equal to

$$E_{1y} = -\frac{U}{\ln(b/a)}\frac{d}{b^2} = -\frac{d}{b}E_t \tag{3.7}$$

in first order of d/b, the ratio of the wire displacement to the tube radius. E_b is the magnitude of the unperturbed field at the wall.

The drift time measured for a track across the tube will be unaffected by the wire displacement only if the track is oriented along $\hat{y}$ so that the nearest electrons travel along $\hat{x}$. The largest effect occurs for electron drift along $\hat{y}$, i.e. the track oriented along $\hat{x}$; for this case we want to compute the apparent track shift Δy.

The measured drift time T is given by the integral over the inverse drift velocity u, where

$$\frac{1}{u} = \frac{1}{\mu E} = \frac{1}{\mu(E_0+E_1)}$$

$$= \frac{1}{\mu E_b \frac{b}{r}\left(1+\frac{d\,r}{b^2}\right)} = \frac{r}{\mu E_b b}\left(1-\frac{d\,r}{b^2}\right) \tag{3.8}$$

to first order in d/b. Therefore,

$$T = \int_0^r \frac{r}{\mu E_b b}\,dr \;-\; \int_0^r \frac{r^2 d}{\mu E_b b^3}\,dr \;= T_0 + \Delta T \tag{3.9}$$

The time shift caused by the wire displacement amounts to

$$|\Delta T| = \frac{dr^3}{3\,\mu E_b b^3}\,, \tag{3.10}$$

and the corresponding coordinate shift is given by

$$\Delta y = u\,\Delta T = \mu E_b \frac{b}{r}\frac{d\,r^3}{\mu E_b b^3} = \frac{d}{3}\frac{r^2}{b^2} \tag{3.11}$$

to first order in d/b. Near the wall, the coordinate shift is one third of the wire displacement, for smaller r it quickly decreases. Δy has the same sign on both sides of the wire, i.e. the track coordinate is displaced in the same direction in which the tube centre has been separated from the wire.

In order to compute the r.m.s. average over many parallel tracks traversing the tube, we replace r by y and let y/b vary between −1 and +1. The average and the variance of the displacement are

$$\langle \Delta y \rangle = d/9 \quad \text{and}$$

$$\left[(\Delta y)^2\right] = \langle (\Delta y)^2 \rangle - \langle \Delta y \rangle^2 = d^2/45 - d^2/81 \tag{3.12}$$

The r.m.s. error is

$$(\Delta y)_{rms} = 0.10\,d. \tag{3.13}$$

3.4.2 Elliptical wall

This case is governed by the small parameter β, where the ratio of the largest to the average tube radii is $1 + \beta$; the ratio of the largest to the smallest tube diameters is then $1 + 4\beta$.

The perturbing quadrupole field has the largest influence for tracks parallel to one of the principal axes of the ellipse. For a track parallel to the $\hat{x}$ direction the drift of the nearest electrons is along $\hat{y}$, and the relevant field component, according to (1.48), is

$$E_{2y} = \beta \frac{U}{\ln (R/a)} \frac{2y}{R^2} = E_R \beta \frac{2y}{R} \qquad (y > 0) \tag{3.14}$$

to first order in β. Here E_R designates the (unperturbed) field at the tube wall.

The inverse of the drift velocity along $\hat{y}$ takes, in first order of β, the form

$$\frac{1}{u} = \frac{1}{\mu E} = \frac{1}{\mu (E_0 + E_2)}$$

$$= \frac{1}{\mu E_R \frac{R}{y}\left(1+\beta\frac{2y^2}{R^2}\right)} = \frac{y}{\mu E_R R}\left(1-2\beta\frac{y^2}{R^2}\right) \tag{3.15}$$

The time shift caused by the deformation is, analogously to (3.10),

$$\Delta T = -2\beta\frac{1}{\mu E_R R}\frac{y^4}{4R^3} \tag{3.16}$$

The corresponding coordinate shift is

$$\Delta y = |u|\left|\Delta T\right| = \mu E_R \frac{R}{y}\frac{\beta}{2}\frac{1}{\mu E_R}\frac{y^4}{R^3} = \frac{\beta}{2}\frac{y^3}{R^2}, \tag{3.17}$$

this shift changes sign at the wire. The average and the variance of the displacement are

$$<\Delta y> = 0$$

$$\left[(\Delta y)^2\right] = <(\Delta y)^2> = \frac{(\beta R)^2}{28}$$

The r.m.s. error is

$$(\Delta y)_{rms} = 0.19\ \beta R. \tag{3.18}$$

For example, an elliptical tube having a difference between largest and smallest diameters of 100 μm will cause an r.m.s. measuring error of 5 μm. Tracks that are not parallel to one of the axes of the ellipse suffer even less.

3.4.3 Hexagonal wall

Let the hexagon be oriented with the largest diameter along $\hat{x}$ and the smallest along $\hat{y}$. The tracks oriented along $\hat{x}$ ($\phi = 0°$), $\phi = 60°$ and 120° will be pulled towards the wire by a shift Δy, and the tracks oriented at $\phi = 30°$, 90° and 150° will be pushed away from the wire by the same amount. In between, the tracks along $\phi = 15°$, 45°, 75°, 105°, 135° and 165° will not be shifted. It is our task to compute Δy as a function of ε, compare (1.50).

The disturbing field component, according to (1.59), and using $\phi = 90°$, is, in first order of ε

$$E_{2y} = \frac{U}{\ln(R/a)} \frac{6\varepsilon}{R} \left(\frac{y}{R}\right)^5 = 6\varepsilon E_R \left(\frac{y}{R}\right)^5 \qquad (y>0) \tag{3.19}$$

E_R is again the magnitude of the unperturbed field at the wall (this quantity was also called $|E_0(R)|$ before). The disturbing field quickly reduces with r.

The inverse of the drift velocity along $\hat{y}$ now takes the form

$$\frac{1}{u} = \frac{1}{\mu(E_0+E_6)} = \frac{1}{\mu E_{R_y} \frac{R}{\left(1+6\varepsilon\left(\frac{y}{R}\right)^6\right)}} = \frac{y}{\mu E_R R}\left(1-6\varepsilon\left(\frac{y}{R}\right)^6\right) \tag{3.20}$$

The time shift caused by the hexagonal shape is, analogously to (3.10),

$$\Delta T = -\frac{6\varepsilon}{\mu E_R}\int_0^y \frac{y^7}{R^7}dy = -\frac{6\varepsilon}{\mu E_R}\frac{y^8}{8R^7} \tag{3.21}$$

The corresponding shift in space equals

$$\Delta y = |u||\Delta T| = \frac{6}{8}\varepsilon R\left(\frac{y}{R}\right)^7 \tag{3.22}$$

This shift also changes sign at the wire. The average and the variance are

$$<\Delta y> = 0$$

$$\left[(\Delta y)^2\right] = \left(\frac{6}{8}\varepsilon R\right)^2 \frac{1}{15} \tag{3.23}$$

The r.m.s. error is

$$(\Delta y)_{rms} = 0.2\,\varepsilon R \tag{3.24}$$

It should be noted that this result is not very accurate, for two reasons. The large size of the distortion makes the neglected second-order terms quite large — for example in (3.20) the neglected terms are of order $(6\varepsilon)^2 \approx 0.1$, or 30% of the retained first order terms. But also the very values of ε and δ (see (1.50)), computed for a geometrical hexagon, are in doubt for a thin plastic foil, and are sensitive to the production process as well as to the gas pressure.

Applying (3.24) to the example of R = 1.5 cm, we obtain an error of approximately ±150 μm. There is a possibility of reducing the error by sacrificing some sensitive space near the wall. Let $\eta = y_{cutoff} / R$ define a cut-off parameter. By restricting the calculation of (3.24) to values $y < y_{cutoff}$ we find

$$(\Delta y^{\text{restricted}})_{rms} = 0.2\,\varepsilon R\,\eta^{7.5} \tag{3.25}$$

For example, a reduction by a factor of 3 is obtained by cutting at $\eta = 0.86$. It should be stressed that the effective radius must still be stable and well known.

3.5 Uncertainty in the coordinate measurement caused by variations in the gas density

It is characteristic of drift tubes that the drift velocity u varies with the gas density ρ over a good part of the radius. This is due to the fact that the dependence of u on ρ and on the electric field E is through the ratio E/ρ. At a fixed wire potential a variation Δρ changes the ratio E/ρ and with it, usually, the drift velocity. In the region near the tube wall where E is small and the electron mobility μ approximately independent of E we can calculate how u varies with ρ. Looking at Fig. 3.7 we observe that u(ρ,E) is completely determined in the domain of

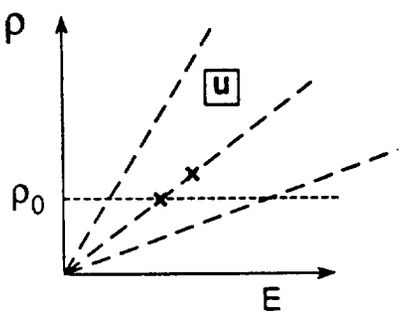

Fig. 3.7. Plane of the two variables E and ρ

ρ and E where u is a function only of E/ρ and where, at some fixed ρ_0, $u = E\,\mu(\rho_0)$. At an arbitrary point (ρ, E), u obviously assumes that value along the line ρ_0 that belongs to the same value of the ratio E/ρ:

$$u(\rho,E) = E_1\,\mu(\rho_0);\quad E_1/\rho_0 = E/\rho, \text{ or}$$

$$u(\rho,E) = \frac{E\,\rho_0}{\rho}\,\mu(\rho_0) \quad . \tag{3.26}$$

We want to compute the shift Δr in the measured coordinate, caused by a change $\Delta\rho$ of the density. We do this under the simplifying condition (2.1, 2.2); this corresponds to the case $r_0 = 0$, a pessimistic one.

The relation between drift time T, position r and density ρ is

$$T(r,\rho) = \int_0^r \frac{r\,dr}{b\,E_b\,\mu(\rho_0)\,(\rho_0/\rho)} = \frac{r^2}{2bE_b\,\mu(\rho_0)}\frac{\rho}{\rho_0} \tag{3.27}$$

Therefore, at a fixed drift time,

$$\Delta T = \frac{\partial T}{\partial r}\,\Delta r + \frac{\partial T}{\partial \rho}\Delta\rho = 0 \quad ;$$

this yields

$$\frac{\Delta r}{r} = -\frac{1}{2}\frac{\Delta\rho}{\rho} \quad . \tag{3.28}$$

The r.m.s. averaging over the radii from 0 to b results in an error of

$$(\Delta r)_{rms} = b\,(\Delta\rho/\rho)\,\left(1/\sqrt{12}\right) . \tag{3.29}$$

For example, if in a tube with radius b = 15 mm the r.m.s. coordinate shift is to stay below 25 μm, the knowledge of the gas density must be better than $(\Delta\rho/\rho) = 0.5\%$.

3.6 Note on averaging the accuracy over the tube

The measurement accuracy of a track varies as a function of the distance x to the wire. When computing 'the measurement accuracy of a tube' there has to be some averaging over x. There are several possibilities, depending on how one wants to determine the track parameters.

The usual situation is such that n tubes are grouped together and a track coordinate x is determined from the few coordinates x_i (i = 1, 2, .. n) measured in the tubes of each group.

The first possibility is to take the simple average

$$x = \frac{1}{n} \sum x_i \, . \tag{3.30}$$

If no further information about the relative positions of the tubes or the orientation of the track is given, we should assume that (A) all parts of the drift space are equally probable, and that (B) the x_i are uncorrelated. These assumptions are appropriate for the early planning stage of an experiment: each tube is characterized by an average accuracy σ_i^*, and a group of n identical tubes yields the accuracy

$$\sigma_{group} = \sigma_i^* / \sqrt{n} \, . \tag{3.31}$$

In order to compute the σ_i^* we evaluate the variance [xx] of (3.30) using the fact that all the x_i have the same expectation value $< x_i >$.

$$[xx] = < x^2 > - < x >^2 = (< (x_1 + x_2 + ..)^2 > - < x_1 + x_2 + .. >^2) / n^2$$

$$[xx] = (< x_i^2 > - < x_i >^2) / n \tag{3.32}$$

because, according to assumption (B), $< x_1 x_2 > = < x_1 > < x_2 >$ etc.. Identifying (3.32) with the square of (3.31), we have

$$\sigma_i^{*2} = < x_i^2 > - < x_i >^2 \, . \tag{3.33}$$

The averaging, denoted by brackets $< >$, is over all the tubes and all the tracks in a given sample of track measurements. Under the assumption (A) this is identical to the average over the drift space, in particular

$$\sigma_i^{*2} = \langle x_i^2 \rangle - \langle x_i \rangle^2 = \frac{1}{2R} \int_{-R}^{+R} \sigma_i^2(x)\, dx \ . \tag{3.34}$$

A second possibility is, to improve on (1) by taking

$$x = \frac{1}{n} \sum W_i x_i \ . \tag{3.35}$$

with

$$W_i = \frac{1/\sigma_i^2}{\sum 1/\sigma_i^2} \ .$$

The use of (3.35) in place of (3.30) promises increased track accuracy if large variations of $\sigma_i(x)$ are present — the one tube of the group in which the track happens to pass through a region of x where $\sigma_i(x)$ is particularly small, will determine the track coordinate of the group almost alone. To evaluate the effect one must obviously know the correlations $\langle W_i x_i\ W_j x_j \rangle$ which depend on the track angle and the geometrical staggering of the tubes. The study of this refined error propagation seems to be more appropriate for a later stage of the experiment.

References

[1] A. Bronwell, Advanced Mathematics in Physics and Engineering (McGraw-Hill, New York 1953)

[2] L. Tonks, Particle transport, electric currents and pressure balance in a magnetically immobilized plasma, Phys. Rev. 97, 1443 (1955)

[3] V.K. Ermilova, L.P. Kotenko, G.I. Merzon and V.A. Chechin, Primary specific ionization of relativistic particles in gases, Sov. Phys. - JETP 29, 861 (1969)

[4] F. Lapique and F. Puiz, Simulation of the measurement by primary cluster counting of the energy lost by a relativistic ionizing particle in argon, Nucl. Instr. Methods 175, 297 (1980)

[5] V.K. Ermilova, L.P. Kotenko and G.I. Merzon, Fluctuations and the most probable values of relativistic charged particle energy loss in thin gas layers, Nucl. Instr. Methods 145, 555 (1977)

[6] ATLAS Muon Group, C. Gruhn et al., Report of the HPDT Parameter Group, to come out soon